



HAL
open science

Selective Tautomer Production and Cryogenic Ion Spectroscopy of Radical Cations: The Uracil and Thymine Cases

Franco Molina, Michel Broquier, Satchin Soorkia, Gilles Grégoire, Gustavo Pino

► **To cite this version:**

Franco Molina, Michel Broquier, Satchin Soorkia, Gilles Grégoire, Gustavo Pino. Selective Tautomer Production and Cryogenic Ion Spectroscopy of Radical Cations: The Uracil and Thymine Cases. *Journal of Physical Chemistry A*, 2024, 128 (18), pp.3596-3603. 10.1021/acs.jpca.4c02199 . hal-04739783

HAL Id: hal-04739783

<https://hal.science/hal-04739783v1>

Submitted on 17 Oct 2024

HAL is a multi-disciplinary open access archive for the deposit and dissemination of scientific research documents, whether they are published or not. The documents may come from teaching and research institutions in France or abroad, or from public or private research centers.

L'archive ouverte pluridisciplinaire **HAL**, est destinée au dépôt et à la diffusion de documents scientifiques de niveau recherche, publiés ou non, émanant des établissements d'enseignement et de recherche français ou étrangers, des laboratoires publics ou privés.

Selective Tautomer Production and Cryogenic Ion Spectroscopy of Radical Cations: The Uracil and Thymine Cases

Franco L. Molina,^[a,b,c,d] Michel Broquier,^[d] Satchin Soorkia,^[d] Gilles Grégoire^{[d]†} and Gustavo A. Pino^{[a,b,c]}*

[a] Centro Láser de Ciencias Moleculares, Universidad Nacional de Córdoba. Haya de la Torre y Medina Allende. Pabellón Argentina, Ciudad Universitaria. X5000HUA Córdoba, Argentina.

[b] INFIQC: Instituto de Investigaciones en Físico-Química de Córdoba (CONICET-UNC). Haya de la Torre y Medina Allende. Pabellón Argentina, Ciudad Universitaria. X5000HUA Córdoba, Argentina.

[c] Departamento de Fisicoquímica, Fac. de Ciencias Químicas, Universidad Nacional de Córdoba. Haya de la Torre y Medina Allende. Pabellón Argentina, Ciudad Universitaria. X5000HUA Córdoba, Argentina.

[d] Université Paris-Saclay, CNRS, Institut des Sciences Moléculaires d'Orsay. F-91405 Orsay, France.

Corresponding Authors

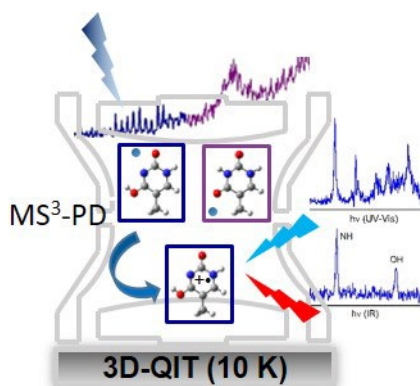
* E-mail: gpino@unc.edu.ar

† E-mail: gilles.gregoire@universite-paris-saclay

ABSTRACT

The vibrational and electronic spectroscopy of the radical cations of two nucleobases (NB) (uracil and thymine) have been studied by cryogenic ion photodissociation spectroscopy. The radical cations have been generated from the photodissociation of NB-Ag⁺ complexes. A charge transfer process from the NB to Ag⁺ governs the deactivation mechanism leading to the formation of the radical cation without further tautomerization. Single and double resonance spectroscopy allows for structural assignments of both the silver complexes and the radical cations by comparison with DFT based calculations. Interestingly, a tautomer-dependent fragmentation is observed in the thymine enol form that involves the loss of NCO, a fragment which was never reported before for this NB. This selective photodissociation of silver complexes containing aromatic chromophore greatly expands the current technique to produce isomer-selected radical cations in the gas phase providing benchmark experimental data to assess calculations of open shell species.

TOC GRAPHICS



KEYWORDS

DNA, radical cations, cryogenic ion spectroscopy, quantum chemistry calculations

Introduction

The coupling of mass-spectrometry to UV photofragmentation spectroscopy¹ has allowed producing and recording the spectroscopy and photodynamics of protonated biomolecules while cryogenic vibrational ion spectroscopy has paved the way to the conformational assignment of mid-sized biomolecules.² More recently, IR spectroscopy coupled to high-resolution ion mobility has been settled to analyse the isomeric complexity of highly flexible systems as glycans,³ but has not yet been applied to radical cations.⁴ Indeed, obtaining detailed information on the electronic structure and energetics of transient species such as radical cations is of general interest to understand the driving force in reaction mechanisms that involve charge transfer processes. The short lifetime and low stability of these reactive species render experimental studies technically challenging.

While neutral nucleobases (NB) have been extensively characterized by different isomer-selective spectroscopies,⁵⁻⁷ the works on their radical cations are limited despite their relevance in several biological processes.⁸ They can trigger proton transfer reactions and tautomerization,⁹ which disrupts the Watson-Crick (WC) hydrogen bonding pattern established for the A-T and G-C pairs, and the subsequent strand scission and mutagenesis.¹⁰ In addition, they could be produced in the Interstellar Medium (ISM) by high energy radiation.^{11,12} Therefore, detailed studies with isomer-selectivity are required in order to reach a better understanding of their intrinsic properties.

Most of the experimental results on the ground and electronically excited states of the NB radical cations have been obtained by excitation of the neutral molecules, and for neutral U and T, the canonical dioxo tautomer is the dominant conformer in the gas phase¹³ and in solution.¹⁴ Cationic vibronic structures of jet-cooled U¹⁵ and T¹⁶ have been accurately determined using tabletop VUV mass-analyzed threshold ionization spectroscopy. The threshold photoelectron spectroscopy

(TPES) of T up to 2 eV above the adiabatic ionization energy was recorded at synchrotron VUV beamlines by Bravaya,¹⁷ Hochlaf^{18,19} and Mayer.²⁰ Broad PES bands are assigned to the excitation of the ground and first excited states of the radical cation and compared to calculated vertical excitation energies.

There are just a few reports dealing with the gas phase electronic spectroscopy of some of the radical cations excited from their corresponding D_0 states. For instance, Dang et al.²¹ generated $T^{+\bullet}$ by dissociation of a Cu-terpyridine-thymine complex in the gas phase and recorded its vis-UV photodissociation spectroscopy. They suggested the formation of a tautomer mixture containing the canonical dioxo isomer along with noncanonical tautomers involving H transfer from the methyl moiety to the adjacent carbonyl group. Although these latter structures are the lowest energy isomers by about 0.2 eV as compared to the canonical form,²² an energy barrier of roughly 1 eV has to be overcome to form these noncanonical tautomers. Finally, the electronic spectroscopic studies were performed at room temperature and without isomer selectivity, which makes the assignment elusive. Readers are referred to recent reviews on the generation and action spectroscopy of DNA and related radical cations.^{23,24}

We have recently developed an original way to produce isomer-selected radical cations of cytosine ($C^{+\bullet}$) in a cold ion trap from the photodissociation of the cytosine- Ag^+ ($C-Ag^+$) complex, that allowed recording high-resolution electronic and vibrational spectroscopy of two different tautomers of $C^{+\bullet}$.²⁵ These results were compared with calculations performed at different levels of theory and establishing benchmark experimental results to improve or develop new theoretical methods for studying the ground and excited states of open-shell species.

The new experimental method is based on the presence of a weakly bound charge transfer state in the $NB-Ag^+$ complex, that lies in the vicinity of the locally excited $\pi-\pi^*$ state and leads to the

photochemical production of the radical cation. The onset of the $\pi-\pi^*$ transition of C-Ag⁺ is observed at 4.32 eV.^{26,27} Taking into account the binding energy (2.86 eV) of the complex and the difference of ionization energies between cytosine C₁ (IE_C = 8.73 eV) and silver atom (IE_{Ag}=7.57 eV), the dissociation limit resulting in the formation of C^{•+} was estimated at 4 eV. The low excess energy (~0.32 eV) deposited in C^{•+} precludes the isomerization/tautomerization, which allows for isomeric selectivity of the radical cation produced.

The goal of this work is to show the universality of this method for studying NB radical cations and very likely any aromatic radical cation, extending the former studies on C^{•+} to the other two pyrimidine bases, thymine (T) and uracil (U) producing their radical cations (T^{•+} and U^{•+}) from the photodissociation of T-Ag⁺ and U-Ag⁺ complexes, respectively and to perform IR and UV cryogenic spectroscopy on them.

Methodology

Experimental Section

The experimental setup in Orsay has already been described in detail.^{25,28} It is based on an electrospray ion source, a cryogenic cooled 3D quadrupole ion trap (QIT, Jordan TOF Inc) and a homemade linear time-of-flight mass spectrometer. A water/methanol solution (1: 1) of a nucleobase (NB) (200 μ M) and AgNO₃ (100 μ M) is electrosprayed in front of a heated capillary. The as produced ions are then transferred into an octopole through a skimmer and stored for 100 ms. A bunch of ions is extracted from the octopole by a pulsed electrode and accelerated at 200 V. NB-Ag⁺ complex ions are mass-selected by a Linear Quadrupole mass filter located in front of the QIT biased at 200 V and mounted on a cold head of a compressed helium cryostat (CH-204S, Sumitomo) that maintains the temperature around 15 K. The mass-selected complexes are stored

and thermalized through collisions with helium buffer gas injected by a pulsed valve (Parker, general valve) a few ms before the entering of the ions. Parent ions and photofragments, as described below, are mass-analyzed in a linear TOF-MS and detected by micro-channel plates (Z-Gap, Jordan TOF Inc.).

Vis/UV lasers and an IR-OPO laser were used for the photo-dissociation spectroscopy. UV photodissociation of NB–Ag⁺ complexes is performed by shining the output of a ps OPA laser (EKSPLA PG 411, 8–10 cm⁻¹ bandwidth) and detecting the nucleobase radical cation fragment (NB^{•+}). The wavelength of the OPA laser can be tuned from 840 nm to 420 nm in the visible with a hole between 740 nm and 680 nm. SHG is then generated to produce the UV light from 420 nm to 210 nm with a hole from 370 nm to 340 nm. To record the spectroscopy of NB^{•+}, the photodissociation laser arrives first at the early beginning of the trapping sequence (3 ms) when NB–Ag⁺ complexes are already cooled, and the relative pressure of the helium in the QIT is still high enough to cool the nascent NB^{•+} photofragment efficiently. An auxiliary RF (1–2 V during 2 ms after the photodissociation laser) whose frequency is tuned in resonance with the mass of the NB–Ag⁺ complex is sent to the entrance endcap of the QIT to eject the remaining complex to ensure the mass-selection of the NB^{•+}.²⁹ Then, a second UV laser arrives about 60 ms later to record the photodissociation spectroscopy of the cooled radical cation.

To record the IR signature of isomer-selected species, two kinds of IR–UV double resonance spectroscopy has been performed depending on the vibronic pattern of the UV spectrum. For species that show sharp vibronic transitions, IR–UV_{on} dip spectroscopy is used, i.e. a tunable OPO IR laser (Laserspec) excites the ions a few 100 ns before the UV photodissociation laser whose frequency is set on the band origin of the UV spectrum. When the ions are selectively excited by the IR laser, the UV photo-fragmentation yield is reduced by the depletion of its ground vibrational

state. When the UV spectroscopy exhibits a broad absorption band, IR–UV_{off} gain spectroscopy is chosen, i.e. the tunable IR laser still arrives at the interaction region a few 100 ns before the UV laser whose frequency is, in this case, set off-resonance in the red of the onset of the absorption band (red-shifted by a few nm). In that case, the resonant absorption of the IR photon heats the molecules, which can now absorb the UV_{off} photon and triggers photo fragmentation. It is noteworthy that this latter method is very sensitive since it allows detecting the IR absorption on a background free UV signal. The IR-UV dip spectroscopy and the IR-UV gain spectroscopy will be called IR-UV_{on} and IR-UV_{off} spectroscopy, respectively.

Theoretical

The ground state equilibrium geometries and frequencies of NB-Ag⁺ complexes and NB⁺⁺ were calculated at the restricted and unrestricted DFT CAM-B3LYP/aug-cc-pVDZ level, respectively, as implemented in Gaussian16.³⁰ Stuttgart effective core potential is used for the silver atom.³¹ The harmonic frequencies were corrected with a global scaling factor of 0.947. Excited state optimizations and frequency calculations of the NB-Ag⁺ complexes have been calculated at the spin-component scaled SCS-CC2 level with correlation-consistent polarized valence double- ζ aug-cc-pVDZ basis set augmented with diffuse functions as implemented in TURBOMOLE program package (v7.1),³² making use of the resolution-of-the-identity (RI) approximation for the evaluation of the electron-repulsion integrals. In the case of NB⁺⁺ isomers, excited state optimizations and frequency calculations were performed at the TD-DFT level with the same functional and basis set for the ground state. Finally, electronic spectra were simulated using the PGOPHER software³³ for Franck Condon analysis.

Results and Discussion

Spectroscopy of Uracil-Ag⁺ Complex

The U-Ag⁺ complex was prepared in an ESI source, guided to and isolated in a cold Quadruple Ion Trap (QIT), where it was cooled down to 15 K and subsequently interrogated by different lasers, as explained in the experimental methodology section. Upon UV excitation of the U-Ag⁺ complex, three fragmentation channels were observed: U⁺⁺ (m/z 112), [UAg-HNCO]⁺ (m/z 176/178) and Ag⁺ (m/z 107/109), the first one being the most intense fragment, as shown in Figure S1.

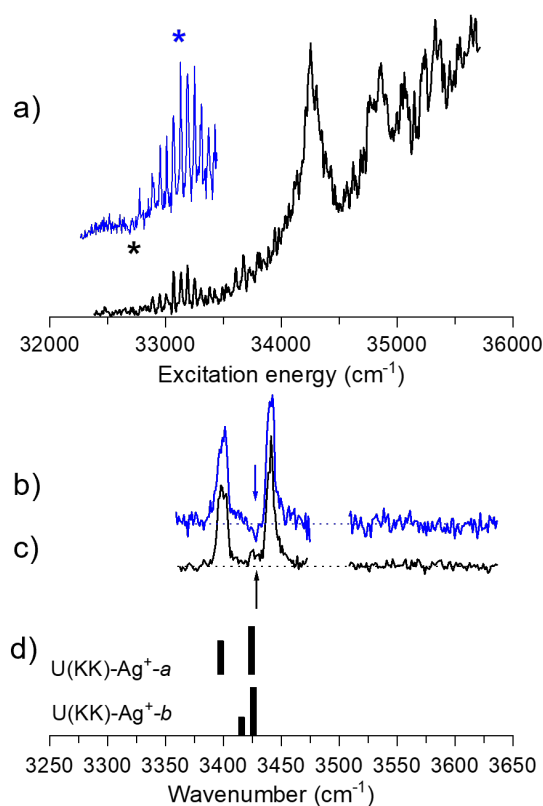


Figure 1. (a) UV photodissociation spectrum of U-Ag⁺ complex in 32000-35500 cm⁻¹, recorded on the U⁺⁺ mass channel. The inset shows a higher resolution spectrum of the first band. (b) IR-UV on spectrum (blue line) with the UV laser at 33063 cm⁻¹ (*). (c) IR-UV off spectrum (black line) with the UV laser at 32700 cm⁻¹ (*). (d) Calculated vibrational spectra of the silver complexes containing U(KK).

The photodissociation spectrum of the U-Ag⁺ complex recorded on the U⁺ (m/z 112) fragment is depicted in Figure 1a. It exhibits two distinct absorption bands. The first band starting at 32770 cm⁻¹ is weak and has well-resolved transitions, displaying a vibrational progression of 60 cm⁻¹, assigned to in-plane wagging mode of Ag (Figure S2) that extends for 750 cm⁻¹. The second band in the 34000 – 36000 cm⁻¹ region is broader and six times more intense than the first band.

The IR-UV_{off} spectrum recorded using the UV laser off-resonance at 32700 cm⁻¹ is dominated by a gain signal as depicted in Figure 1.c. This spectrum exhibits three vibrational transitions in the NH stretching mode region: two intense transitions at 3400 cm⁻¹ and 3441 cm⁻¹ and a small shoulder around ~3425 cm⁻¹. The IR-UV_{on} spectrum (Figure 1b) with the UV laser on-resonance at 33063 cm⁻¹ shows gain signals for the two intense transitions, while the shoulder at ~3425 cm⁻¹ appears as a dip signal, indicating that the last one corresponds to a different isomer, which in turns is the isomer that resonantly absorbs at the UV photon energy (33063 cm⁻¹). Neither the IR-UV_{off} nor the IR-UV_{on} spectra show any transition in the OH stretching mode region, which allows excluding the keto-enol (KE) tautomers. To conclude, two keto-keto (KK) tautomers are responsible for the observed transitions. Therefore, the structures of the two possible isomers of the U(KK)-Ag⁺ complex, which differ only by the orientation of Ag⁺ around the oxygen, were optimized at the CAM-B3LYP/aug-cc-pVDZ (CHON) and SDD (Ag) level of theory and their corresponding IR spectra were also calculated at the same level, as shown in Figure 1d.

According to the calculated IR spectra, the strong transitions at 3400 cm⁻¹ and the weak transition at 3425 cm⁻¹ are assigned to the N₍₃₎H stretching vibration modes of the U(KK)-Ag⁺-*a* and the U(KK)-Ag⁺-*b* isomers, respectively, while the transition observed at 3441 cm⁻¹ is assigned to the

$N_{(1)}H$ stretching mode of both isomers (Figure 1.d). See Scheme 1 in supporting information for the atom labelling.

The isomers contribution to the first electronic transition (32770-33500 cm^{-1}) was analyzed by UV-UV HB spectroscopy probing the vibronic transition at 33063 cm^{-1} . As shown in Figure S3, all the vibronic transitions are depleted confirming the contribution of a single isomer. Thus, this band is assigned to the U(KK)-Ag⁺-*b* isomer while the second intense and broad band is assigned to the U(KK)-Ag⁺-*a* isomer and probably a contribution of the U(KK)-Ag⁺-*b* isomer as well.

The vertical (E_v) and adiabatic (E_{ad}) excitation energies of the two U(KK)-Ag⁺ isomers, corrected by the zero-point energy (ΔZPE) difference between the ground and excited states are reported in Table S1. The excited state optimization and $E_{ad} + \Delta ZPE$ calculations were performed only for the two first A' transitions ($n-\sigma^*$ and $\pi-\pi^*$ in Cs symmetry) that have sizeable oscillator strengths (f). As shown in Table S1, the $E_{ad} + \Delta ZPE$ for the first $n-\sigma^*$ transition of both isomers is calculated in the 33000 cm^{-1} region in agreement with the band origin (BO) of the first experimental band, while the corresponding values for the $\pi-\pi^*$ transition of both isomers are calculated at higher energies ($\sim 35500 \text{ cm}^{-1}$) and with a larger oscillator strength which is in line with the second experimental band.

According to the IR-UV_{on} spectroscopy and UV-UV HB spectroscopy on the first band (32770-33500 cm^{-1}) only the $n-\sigma^*$ transition of the U(KK)-Ag⁺-*b* isomer is assigned in this excitation region. In contrast, the broad absorption band starting at about 34000 cm^{-1} could be assigned to $\pi-\pi^*$ transition of both conformers whose calculated adiabatic excitation energies (35541 cm^{-1} and 35736 cm^{-1} for U(KK)-Ag⁺-*a* and U(KK)-Ag⁺-*b*, respectively) are in fair agreement with the experimental value. It should be stressed here that although two conformers of U-Ag⁺ are present,

solely the dioxo uracil tautomer U(KK) forms the complexes whose structures only differ by the orientation of the silver cation around the carbonyl group.

Spectroscopy of U⁺

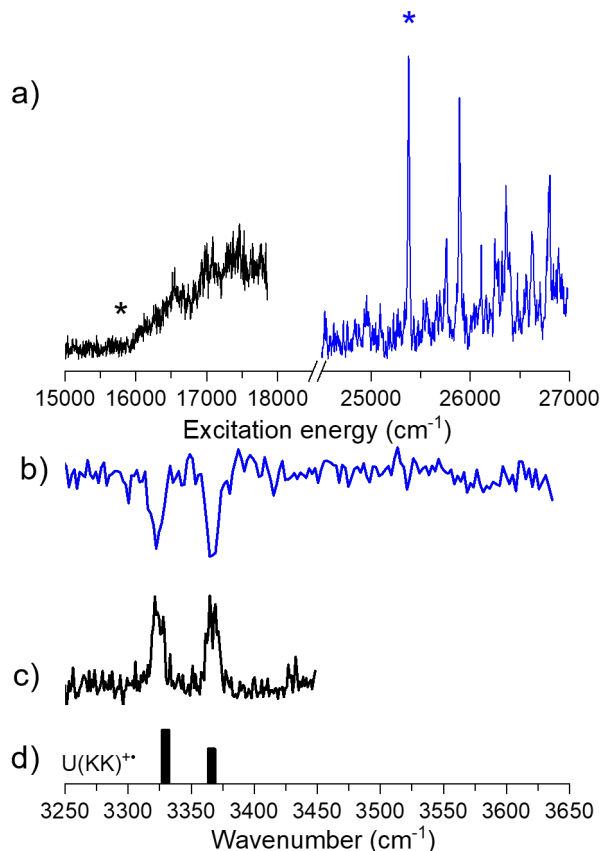


Figure 2. (a) Photodissociation spectrum of U⁺ issued from the photodissociation of the U-Ag⁺ complex at 34125 cm⁻¹ and recorded on the HNCO loss mass channel. The inset (light-grey line) shows the FC simulation of the D₀→D₄ transition for U(KK)⁺. (b) IR-UV_{on} spectrum (blue line) with the UV laser at 25377 cm⁻¹ (blue star). (c) IR-Vis_{off} spectrum (black line) with the UV laser at 15700 cm⁻¹ (black star). (d) Calculated vibrational spectra of the U(KK)⁺ isomer.

To record the spectroscopy of U⁺, a first laser was used to photodissociate the U(KK)-Ag⁺ complex at 33063 cm⁻¹ (excitation of the U(KK)-Ag⁺-*b* isomer) or at 34125 cm⁻¹ (broad absorption

band). The photofragment $U^{+\bullet}$ was isolated and cooled down in the QIT as explained in the experimental methodology section. Then, the pulse of a second laser enters into the trap to perform the photofragmentation spectroscopy of $U^{+\bullet}$. The HNCO loss channel (m/z 69) was observed upon vis-UV excitation of $U^{+\bullet}$ from 15000 cm^{-1} to 27000 cm^{-1} , as already reported for this species.³⁴

The photofragmentation spectrum of $U^{+\bullet}$ shown in Figure 2a is identical whether the radical cation is produced from the dissociation of either the $U(\text{KK})\text{-Ag}^+\text{-}a$ or $U(\text{KK})\text{-Ag}^+\text{-}b$ conformers. It displays two absorption bands: a broad band with an onset around 16000 cm^{-1} and a set of sharp vibronic transitions with the BO at 25377 cm^{-1} .

The IR-UV_{on} dip and IR-V_{isoff} gain spectra of $U^{+\bullet}$ were recorded with the UV laser set on the BO at 25377 cm^{-1} and to the red of the broad absorption band at 15700 cm^{-1} , and are shown in Figures 2c and 2b, respectively. The two experimental IR spectra are identical, with two vibrational transitions at 3322 cm^{-1} and 3364 cm^{-1} , assigned the $N_{(1)}\text{H}$ and $N_{(3)}\text{H}$ stretching modes, respectively. This IR spectrum is readily assigned to the $U(\text{KK})^{+\bullet}$ tautomer by comparison with its predicted vibrational spectrum (Figure 2d). It can be concluded that the structure of the uracil radical cation is retained following the photodissociation of the $U\text{-Ag}^+$ complex.

Spectroscopy of Thymine- Ag^+ Complex

Upon UV excitation of the $T\text{-Ag}^+$ complex, two fragmentation channels were observed: the most intense m/z 126 ($T^{+\bullet}$) along with weak signals at m/z 107/109 (Ag^+) as shown in Figure S4. The photodissociation spectrum of the $T\text{-Ag}^+$ complex recorded on the $T^{+\bullet}$ (m/z 126) fragment is shown in Figure 3.a. Two distinct absorption bands are observed: the first weak band starts at 32280 cm^{-1} with a well resolved vibronic progression of 50 cm^{-1} , assigned to the in-plane wagging mode of Ag (Figure S5) that extends for 500 cm^{-1} . The second band in the $33250 - 35250\text{ cm}^{-1}$ region is

broader and more intense than the first band. In overall, the excitation spectrum of T-Ag⁺ shares many similarities with the ones recorded for U-Ag⁺ and C-Ag⁺.²⁵ So, one might expect to observe only the KK isomers of T-Ag⁺ complex as for the two other pyrimidine nucleobases. However, as it will be discussed below, the KE tautomer also contributes to the experimental spectrum.

The IR-UV_{off} and IR-UV_{on} spectra recorded with the UV laser set at different wavelengths are shown in Figures 3b and 3c, respectively. The IR-UV_{off} (black line) spectrum comprises three vibrational transitions in the NH stretching mode region (3395 cm⁻¹, 3430 cm⁻¹ and 3442 cm⁻¹) and two other vibrational transitions in the OH stretching mode region (3585 cm⁻¹ and 3594 cm⁻¹). These numerous vibrational transitions suggest the presence of multiple KK and KE isomers. The IR-UV_{on} spectrum (blue line) with the UV laser set at 32504 cm⁻¹ shows only two vibrational bands depleted at 3430 cm⁻¹ and 3594 cm⁻¹, corresponding to a single NH and a single OH stretching modes, respectively and thus, assigned to a KE tautomer. The IR-UV hole burning spectrum (Figure S6) recorded by setting the burn IR laser at 3594 cm⁻¹ while scanning the UV laser in the sharp vibronic band region around 32500 cm⁻¹ confirms that a single KE tautomer contributes to the excitation spectrum of T-Ag⁺ in this spectral range. All the IR-UV spectra, whatever the UV probe wavelength, are dominated by gain signals suggesting that at least another KE and one KK isomer contribute to the broad absorption band above 33000 cm⁻¹.

The calculated structure of two T(KK)-Ag⁺ and two T(KE)-Ag⁺ isomers are shown in Figure 3d. The calculated IR spectra for the two KE rotamers are very similar. Their calculated NH and OH stretch frequencies match the experimental transitions. For T(KEr)-Ag⁺ conformer, the OH stretching frequency is slightly blue shifted as compared with T(KE)-Ag⁺ conformer, suggesting that the former conformer could be assigned to the IR dip signal observed while probing the sharp UV transitions at 32500 cm⁻¹. Nevertheless, the two NH and OH stretching modes are very close,

both experimentally and theoretically, so a definitive assignment is still difficult, but in any case thymine is in the KE form.

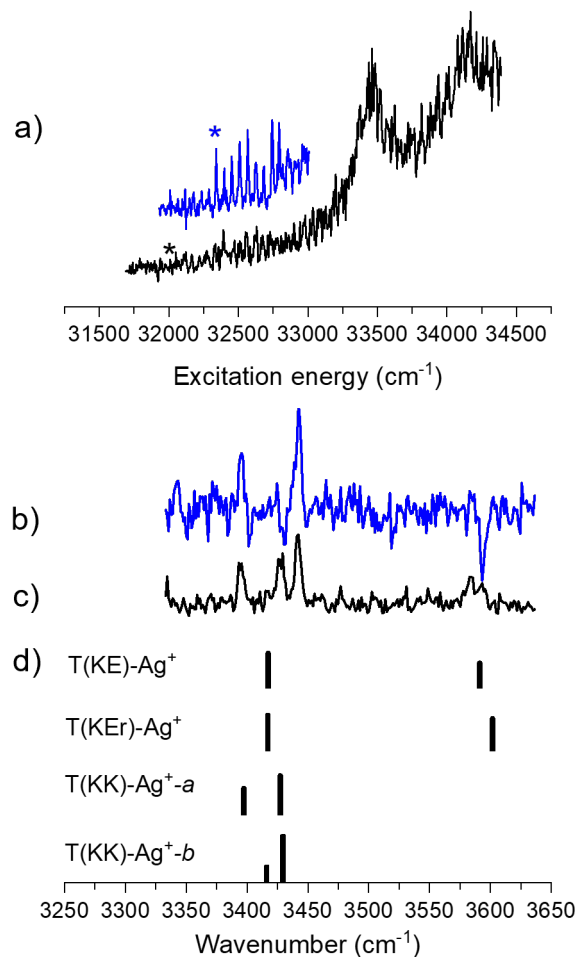


Figure 3. (a) UV photodissociation spectrum of T-Ag⁺ complex in 31500-34750 cm⁻¹, recorded on the T⁺ mass channel. The inset shows a higher resolution spectrum of the first band. (b) IR-UV_{on} spectrum (blue line) with the UV laser at 32504 cm⁻¹ (*). (c) IR-UV_{off} spectrum (black line) with the UV laser at 32200 cm⁻¹ (*). (d) Calculated vibrational spectra of four isomers of the T-Ag⁺ complex.

The other two gain transitions observed in both, the IR-UV_{on} and IR-UV_{off} spectra (Figures 3b and 3c) at 3395 cm⁻¹ and 3442 cm⁻¹, corresponding to the NH stretching modes, are satisfactorily reproduced in the calculated spectrum of T(KK)-Ag⁺-a conformer, while the frequency splitting calculated for T(KK)-Ag⁺-b conformer is smaller. So these two transitions could be reasonably

assigned to the former KK-*a* conformer. However, the presence of the KK-*b* conformer cannot be ruled out since the calculated NH stretch frequencies (3433 cm^{-1} and 3445 cm^{-1}) for this isomer are in agreement with some of the experimental transitions.

The vertical excitation energies E_v were calculated for the first four electronically excited states of all isomers and are reported in Table S2. The electronic states with $n-\sigma^*$ and $\pi-\pi^*$ character (A' transitions) have the highest oscillator strengths and thus, these states were further optimized and the $E_{ad}+\Delta ZPE$ were calculated to compare with the experimental values. The $E_{ad}+\Delta ZPE$ calculated for the $n-\sigma^*$ transition of any of the KE isomers is in good agreement with the BO of the first band (32280 cm^{-1}), while the corresponding values for the $\pi-\pi^*$ transition is calculated in the region of the second broad band. The spectral region of the second band is also in agreement with the $E_{ad}+\Delta ZPE$ calculated for the $n-\sigma^*$ of both KK isomers. These results, are in line with the assignment done based on the IR spectroscopy. Finally, the $\pi-\pi^*$ transition of the KK-*a* isomer could also contribute to the higher energy side of the second broad band.

The variety of isomers identified for the T- Ag^+ complex that can be excited simultaneously in the second absorption band renders the selective photochemical preparation of T^{++} impossible. Therefore, we will first present the spectroscopy of T^{++} produced from the selective dissociation of the T(KE)- Ag^+ tautomer.

Spectroscopy of T^{++} issued from the photodissociation of the T- Ag^+ complex at 32500 cm^{-1}

The photofragmentation spectrum of T^{++} resulting from the photodissociation of any of the T(KEr)- Ag^+ /T(KE)- Ag^+ complexes at 32500 cm^{-1} exhibits two set of bands: a first broad absorption band in the visible region ($14000\text{-}22000\text{ cm}^{-1}$) and a second absorption band in the near UV region, with a few vibronic transitions starting at 24857 cm^{-1} (BO) and extending up to 27000

cm^{-1} , Figure 4a. In the visible range, only one fragmentation channel was detected at m/z 83 corresponding to the loss of HNC. However, in the near UV, in addition to m/z 83, two other fragmentation channels are observed at m/z 84 (NCO loss) and m/z 55 (HNC + CO loss).

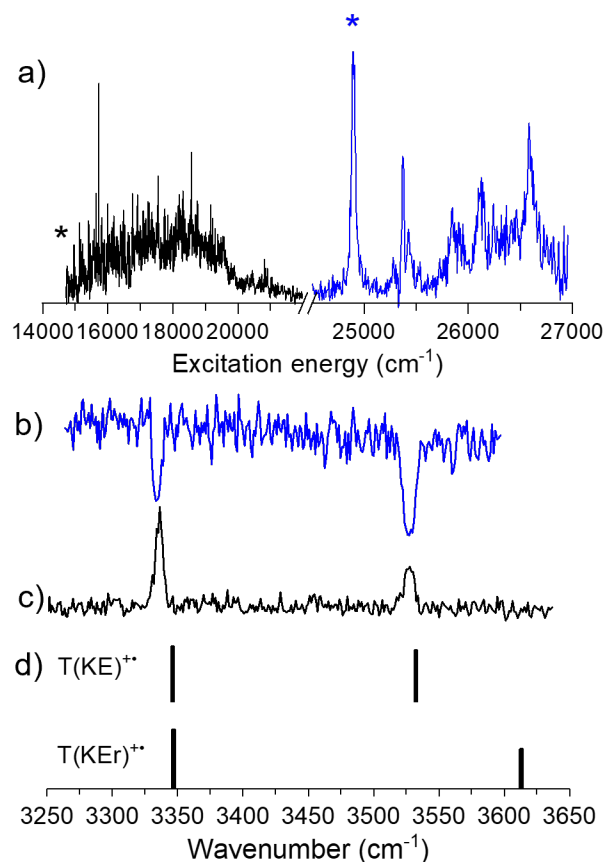


Figure 4. (a) Photodissociation spectroscopy of T^{+} issued from the photodissociation of T-Ag^{+} at 32500 cm^{-1} monitoring the fragmentation channel m/z 83 (black line in the visible region) and the fragmentation channel m/z 84 (blue line in the near UV region). The inset (light-grey line) shows the FC simulation of the $\text{D}_0 \rightarrow \text{D}_4$ transition for T(KE)^{+} . (b) IR- UV_{on} spectrum (blue line) with the UV at 24857 cm^{-1} (blue star). (c) IR- UV_{off} spectrum (black line) with the UV laser at 14700 cm^{-1} (black star). (d) Calculated vibrational spectra of T(KE)^{+} isomers.

The IR- UV_{on} dip spectrum probing the BO of the second absorption band is shown in Figure 4b. Two vibrational bands at 3335 cm^{-1} and 3527 cm^{-1} are observed in the NH and OH stretching region, respectively, suggesting that this is the T(KE)^{+} tautomer. The IR- Vis_{off} gain spectrum

(Figure 4c) probing the visible band exhibits the same two IR transitions, revealing that the entire electronic spectrum can be assigned to the same isomer. The comparison with the calculated IR spectra for both T(KE)⁺⁺ and T(KEr)⁺⁺ rotamers (Figure 4d) allows assigning the spectral features to the T(KE)⁺⁺ conformer, due to the better agreement in the OH stretching mode region. Once more, the preparation of the radical cation from the photofragmentation of the corresponding complex with Ag⁺ preserves the tautomeric identity of the base.

Spectroscopy of T⁺⁺ issued from the photodissociation of the T-Ag⁺ complex at 34500 cm⁻¹

When T⁺⁺ is produced from the photodissociation of the T-Ag⁺ complex at 34500 cm⁻¹, several isomers of T-Ag⁺ containing either T(KE) or T(KK) tautomers are electronically excited. The photofragmentation spectrum of T⁺⁺, recorded on the fragmentation channel m/z 83 (HNCO loss) shows two set of bands as depicted in Figure 5a. A broad absorption band starting below 15000 cm⁻¹ and a second band in the UV spectral region constituted by a set of well-resolved vibronic transitions with a BO at 25773 cm⁻¹ and another very weak transition at 24857 cm⁻¹. The weak transition at 24857 cm⁻¹ is assigned to the BO of the near UV band of the T(KE)⁺⁺ isomer. Other fragments were also observed and they are discussed in the SI.

The IR-Vis_{off} gain spectrum recorded with the probe laser set at 14700 cm⁻¹ (Figure 5c) shows two vibrational transitions at 3335 cm⁻¹ and 3371 cm⁻¹, in the NH stretch region, and a third vibrational transition at 3527 cm⁻¹ in the OH region. The IR-UV_{on} dip spectrum recorded probing the BO at 25773 cm⁻¹ (Figure 5b) shows only two vibrational transitions at 3335 cm⁻¹ and 3371 cm⁻¹ assigned to the N₍₁₎H and N₍₃₎H stretching modes of the KK tautomer.

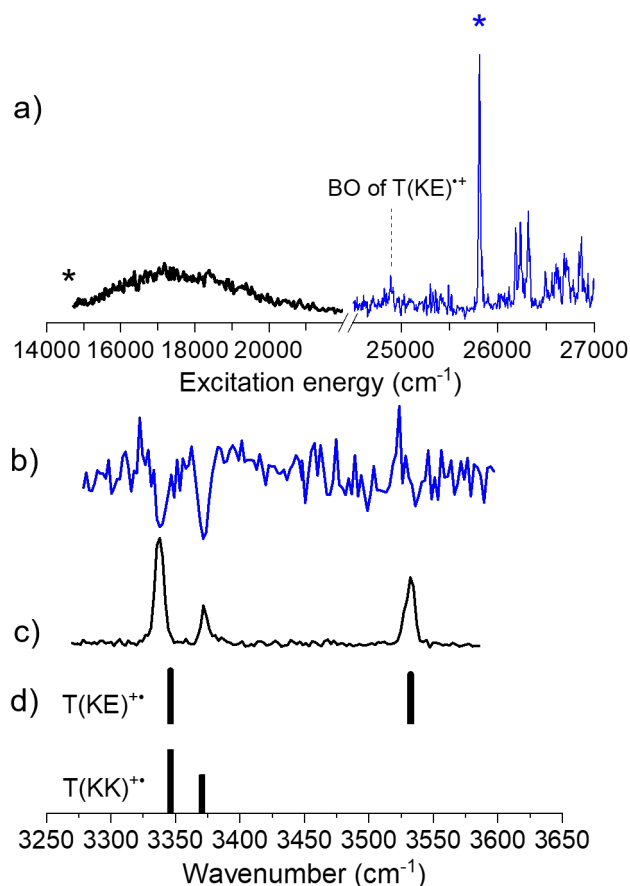


Figure 5. (a) Photodissociation spectroscopy of T^{++} issued from the photodissociation of $T\text{-Ag}^+$ at 34500 cm^{-1} , monitoring the fragmentation channels m/z 83. The inset (light-grey line) shows the FC simulation of the $D_0 \rightarrow D_4$ transition for $T(\text{KK})^{++}$. (b) IR- UV_{on} spectrum (blue lines) with the UV at 25773 cm^{-1} (blue star). (c) IR- UV_{off} spectrum (black lines) with the UV at 14700 cm^{-1} (black star). (d) Calculated vibrational spectra of the $T(\text{KE})^{++}$ and $T(\text{KK})^{++}$ isomers.

By comparison with the calculated spectra (Figure 5d) and the IR spectrum of the $T(\text{KE})^{++}$ isomer reported in the previous section, the band at 3527 cm^{-1} is assigned to the OH stretch of this isomer, while the band at 3335 cm^{-1} is assigned to the $\text{N}_{(1)}\text{H}$ stretch of both isomers.

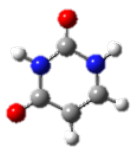
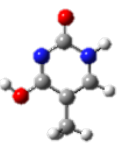
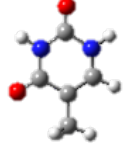
Therefore, the UV band with the BO at 25773 cm^{-1} is assigned to the $T(\text{KK})^{++}$ tautomer, while the broad band in the visible region is assigned to both, $T(\text{KK})^{++}$ and $T(\text{KE})^{++}$ tautomers. These

results confirm that at least two isomers of T-Ag⁺ containing T(KK) and T(KE) absorb at 34500 cm⁻¹.

The calculated vertical and adiabatic transition energies of the A' transitions of U(KK)⁺⁺, T(KK)⁺⁺ and T(KE)⁺⁺ are reported in Table 1. The calculated E_{ad}+ΔZPE of the D₀ → D₄ transitions for all the isomers are in fair agreement with the experimental BO of the sharp vibronic transitions observed at 25377 cm⁻¹ for U(KK)⁺⁺, 24857 cm⁻¹ for T(KE)⁺⁺ and 25773 cm⁻¹ for T(KK)⁺⁺. To confirm the assignment of the three vibronic spectra recorded in the 25000 cm⁻¹ spectral region, the Franck-Condon simulations of the D₀ → D₄ transition of U(KK)⁺⁺, T(KE)⁺⁺ and T(KK)⁺⁺ were performed and compared with the experimental vibronic spectra as reported in Figure 2a, Figure 4a and Figure 5a, respectively. For all species, a very good agreement with the experimental spectra is found. This clearly indicates that excited state geometry optimization at the TD-DFT level is quite reliable even for such high transition energy (D₀ → D₄) as it was already reported for C(KK)⁺⁺.²⁵

However, the large error predicted for the first ππ* state (D₀ → D₂) in all species may be explained by the predicted low energy gap with the first and/or second dark nπ* electronic states that lie close in energy to the first ππ* state in each radical cation. A conical intersection (CI) of D₂ with D₀ and D₁ states of U(KK)⁺⁺ and T(KK)⁺⁺, respectively, has been reported in a theoretical work performed at the XMS-CAPT2 level.³⁵ The same mechanism could be at play for T(KE)⁺⁺. For instance, the optimization of the D₂ state of the T(KE)⁺⁺ isomer, whose vertical excitation energy is calculated at 16900 cm⁻¹, did not converge due to the close vicinity with the D₃ state. The close proximity between the first ππ* state and the dark nπ*, is likely to be responsible for the observed broadening in the first electronic transition in the visible region for the three radical cations.

Table 1: Vertical excitation energies (E_v), adiabatic excitation energies corrected by the zero-point energy difference ($E_{ad} + \Delta ZPE$), and oscillator strengths (f) of the four lowest excited states of $U(KK)^{+\bullet}$, $T(KK)^{+\bullet}$ and $T(KE)^{+\bullet}$.^[a] The excited state energies for each species are relative to the ground state. All energies are reported in cm^{-1} .

Isomers	State	E_v	$E_{ad} + \Delta ZPE$	f
 $U(KK)^{+\bullet}$	$D_1 (n_O-\pi^*) (A'')$	9700	-	0
	$D_2 (\pi-\pi^*) (A')$	15202	11066	2×10^{-2}
	$D_3 (n_O-\pi^*) (A'')$	20275	-	0
	$D_4 (\pi-\pi^*) (A')$	33155	27430	3×10^{-2}
 $T(KE)^{+\bullet}$	$D_1 (n-\pi^*) (A'')$	12897	-	0
	$D_2 (\pi-\pi^*) (A')$	16905	*	4×10^{-2}
	$D_3 (n-\pi^*) (A'')$	16938	-	0
	$D_4 (\pi-\pi^*) (A')$	29962	26132	7×10^{-2}
 $T(KK)^{+\bullet}$	$D_1 (n-\pi^*) (A'')$	12700	-	0
	$D_2 (\pi-\pi^*) (A')$	17166	12482	1×10^{-2}
	$D_3 (n-\pi^*) (A'')$	21251	-	0
	$D_4 (\pi-\pi^*) (A')$	32603	26924	6×10^{-2}

[a] CAM-B3LYP/aug-cc-pVDZ level

* not converged due to state crossing.

Conclusions

To conclude, this work reports the cryogenic vibrational and electronic spectroscopy of uracil and thymine radical cations generated from the photodissociation of their corresponding NB-Ag⁺ complexes. The charge transfer process occurring in the excited state of the NB-Ag⁺ complex is very efficient since it leads to the formation of NB radical cations as the main photofragment. Besides, NB radical cations are produced without further tautomerization, which thus allows the selective generation of the given tautomer of NB^{+\bullet}. Single and double resonance photodissociation spectroscopies have been recorded at an unprecedented spectral resolution through cryogenic ion spectroscopy. The structures of the radical cations have been determined through comparison with vibrational and vibronic calculations performed at the DFT level. These benchmark experimental

data should be used to assess the quantum chemistry calculations of open-shell species. For thymine, the formation of the rare enol tautomer has allowed to record its vibrational and electronic spectroscopy. A specific photofragment (NCO loss) has been detected and used to record selectively the vibronic spectroscopy of $T(KE)^{+\bullet}$ in the near UV spectral range.

The methodology presented here for producing radical cations with isomeric selection to study their cryogenic spectroscopy, could be relevant in several areas in which extensive and detailed spectroscopy characterization of radical cations is required.

ASSOCIATED CONTENT

The Supporting Information (Tautomer-dependent fragmentation of T^+ , supplementary Tables and Figures) is available free of charge at <https://pubs.acs.org/doi/>

ACKNOWLEDGEMENTS

This work has been conducted within the International Associated Laboratory LEMIR (CNRS/CONICET) and was supported in part by CNRS, CONICET, FONCyT, SeCyT-UNC, the “ADI 2019” project funded by the IDEX Paris-Saclay, ANR-11- IDEX-0003-02 and ECOS Sud - MinCyT (A22U01) cooperation project. The computations were performed at the HPC resources from the “Mésocentre” computing center of Centra-leSupelec and Ecole Normale Supérieure Paris-Saclay supported by CNRS and Région Ile-de-France (<https://mesocentre.centrale-supelec.fr/>), from the CCAD-UNC and from the HPC resources MAGI from University Paris 13.

REFERENCES

- (1) Soorkia, S.; Juvet, C.; Grégoire, G. UV Photoinduced Dynamics of Conformer-Resolved

- Aromatic Peptides. *Chem. Rev.* **2020**, *120* (7), 3296–3327.
<https://doi.org/10.1021/acs.chemrev.9b00316>.
- (2) Boyarkin, O. V. Cold Ion Spectroscopy for Structural Identifications of Biomolecules. *Int. Rev. Phys. Chem.* **2018**, *37* (3–4), 559–606.
<https://doi.org/10.1080/0144235X.2018.1547453>.
- (3) Ben Faleh, A.; Warnke, S.; Rizzo, T. R. Combining Ultrahigh-Resolution Ion-Mobility Spectrometry with Cryogenic Infrared Spectroscopy for the Analysis of Glycan Mixtures. *Anal. Chem.* **2019**, *91* (7), 4876–4882. <https://doi.org/10.1021/acs.analchem.9b00659>.
- (4) Marlton, S. J. P.; Trevitt, A. J. The Combination of Laser Photodissociation, Action Spectroscopy, and Mass Spectrometry to Identify and Separate Isomers. *Chem. Commun.* **2022**, *58* (68), 9451–9467. <https://doi.org/10.1039/d2cc02101c>.
- (5) De Vries, M. S.; Hobza, P. Gas-Phase Spectroscopy of Biomolecular Building Blocks. *Annu. Rev. Phys. Chem.* **2007**, *58* (1), 585–612.
<https://doi.org/10.1146/annurev.physchem.57.032905.104722>.
- (6) de Vries, M. S. Tautomer-Selective Spectroscopy of Nucleobases, Isolated in the Gas Phase. In *Tautomerism: Methods and Theories*; John Wiley & Sons, Ltd, 2013; pp 177–196.
<https://doi.org/10.1002/9783527658824.ch7>.
- (7) Boldissar, S.; De Vries, M. S. How Nature Covers Its Bases. *Physical Chemistry Chemical Physics*. Royal Society of Chemistry 2018, pp 9701–9716.
<https://doi.org/10.1039/c8cp01236a>.
- (8) Friedberg, E. C. DNA Damage and Repair. *Nature*. 2003, pp 436–440.

<https://doi.org/10.1038/nature01408>.

- (9) Kanvah, S.; Joseph, J.; Schuster, G. B.; Barnett, R. N.; Cleveland, C. L.; Landman, U. Oxidation of DNA: Damage to Nucleobases. *Acc. Chem. Res.* **2010**, *43* (2), 280–287. <https://doi.org/10.1021/ar900175a>.
- (10) Bertran, J.; Blancafort, L.; Noguera, M.; Sodupe, M. Proton Transfer in DNA Base Pairs. In *Computational Studies of RNA and DNA*; Springer Netherlands, 2006; pp 411–432. https://doi.org/10.1007/978-1-4020-4851-3_16.
- (11) Gudipati, M. S.; Allamandola, L. J. Unusual Stability of Polycyclic Aromatic Hydrocarbon Radical Cations in Amorphous Water Ices up to 120 K: Astronomical Implications. *Astrophys. J.* **2006**, *638* (1), 286–292. <https://doi.org/10.1086/498816>.
- (12) Callahan, M. P.; Smith, K. E.; Cleaves, H. J.; Ruzicka, J.; Stern, J. C.; Glavin, D. P.; House, C. H.; Dworkin, J. P. Carbonaceous Meteorites Contain a Wide Range of Extraterrestrial Nucleobases. *Proc. Natl. Acad. Sci. U. S. A.* **2011**, *108* (34), 13995–13998. <https://doi.org/10.1073/pnas.1106493108>.
- (13) Choi, M. Y.; Miller, R. E. Infrared Laser Spectroscopy of Uracil and Thymine in Helium Nanodroplets: Vibrational Transition Moment Angle Study. *J. Phys. Chem. A* **2007**, *111* (13), 2475–2479. <https://doi.org/10.1021/jp0674625>.
- (14) Rejnek, J.; Hanus, M.; Kabeláč, M.; Ryjáček, F.; Hobza, P. Correlated Ab Initio Study of Nucleic Acid Bases and Their Tautomers in the Gas Phase, in a Microhydrated Environment and in Aqueous Solution. Part 4. Uracil and Thymine. *Phys. Chem. Chem. Phys.* **2005**, *7* (9), 2006–2017. <https://doi.org/10.1039/b501499a>.

- (15) Choi, K. W.; Lee, J. H.; Kim, S. K. Vacuum-Ultraviolet Ionization Spectroscopy of the Jet-Cooled RNA-Base Uracil. *Chem. Commun.* **2006**, No. 1, 78–79. <https://doi.org/10.1039/b512465d>.
- (16) Choi, K. W.; Lee, J. H.; Kim, S. K. Ionization Spectroscopy of a DNA Base: Vacuum-Ultraviolet Mass-Analyzed Threshold Ionization Spectroscopy of Jet-Cooled Thymine. *J. Am. Chem. Soc.* **2005**, *127* (45), 15674–15675. <https://doi.org/10.1021/ja055018u>.
- (17) Bravaya, K. B.; Kostko, O.; Dolgikh, S.; Landau, A.; Ahmed, M.; Krylov, A. I. Electronic Structure and Spectroscopy of Nucleic Acid Bases: Ionization Energies, Ionization-Induced Structural Changes, and Photoelectron Spectra. *J. Phys. Chem. A* **2010**, *114* (46), 12305–12317. <https://doi.org/10.1021/jp1063726>.
- (18) Schwell, M.; Hochlaf, M. Photoionization Spectroscopy of Nucleobases and Analogues in the Gas Phase Using Synchrotron Radiation as Excitation Light Source. In *Photoinduced Processes in Nucleic Acids*; 2014; pp 155–208. https://doi.org/10.1007/128_2014_550.
- (19) Hochlaf, M.; Pan, Y.; Lau, K. C.; Majdi, Y.; Poisson, L.; Garcia, G. A.; Nahon, L.; Al Mogren, M. M.; Schwell, M. Vibrationally Resolved Photoelectron Spectroscopy of Electronic Excited States of DNA Bases: Application to the \tilde{A} State of Thymine Cation. *J. Phys. Chem. A* **2015**, *119* (7), 1146–1153. <https://doi.org/10.1021/acs.jpca.5b00466>.
- (20) Majer, K.; Signorell, R.; Heringa, M. F.; Goldmann, M.; Hemberger, P.; Bodi, A. Valence Photoionization of Thymine: Ionization Energies, Vibrational Structure, and Fragmentation Pathways from the Slow to the Ultrafast. *Chem. – A Eur. J.* **2019**, *25* (62), 14192–14204. <https://doi.org/10.1002/chem.201903282>.

- (21) Dang, A.; Nguyen, H. T. H.; Ruiz, H.; Piacentino, E.; Ryzhov, V.; Tureček, F. Experimental Evidence for Noncanonical Thymine Cation Radicals in the Gas Phase. *J. Phys. Chem. B* **2018**, *122* (1), 86–97. <https://doi.org/10.1021/acs.jpcc.7b09872>.
- (22) Nam, J. K. DFT Study of Water-Assisted Intramolecular Proton Transfer in the Tautomers of Thymine Radical Cation. *Bull. Korean Chem. Soc.* **2006**, *27* (7), 1009–1014. <https://doi.org/10.5012/bkcs.2006.27.7.1009>.
- (23) Tureček, F. UV-vis Spectroscopy of Gas-phase Ions. *Mass Spectrom. Rev.* **2023**, *42* (1), 206–226. <https://doi.org/10.1002/mas.21726>.
- (24) Tureček, F. Flying DNA Cation Radicals in the Gas Phase: Generation and Action Spectroscopy of Canonical and Noncanonical Nucleobase Forms. *J. Phys. Chem. B* **2021**, *125* (26), 7090–7100. <https://doi.org/10.1021/acs.jpcc.1c03674>.
- (25) Molina, F.; Dezalay, J.; Soorkia, S.; Broquier, M.; Hochlaf, M.; Pino, G. A.; Grégoire, G. Cryogenic IR and UV Spectroscopy of Isomer-Selected Cytosine Radical Cation. *Phys. Chem. Chem. Phys.* **2022**, *24* (41), 25182–25190. <https://doi.org/10.1039/D2CP03953B>.
- (26) Taccone, M. I.; Féraud, G.; Berdakin, M.; Dedonder-Lardeux, C.; Jouvét, C.; Pino, G. A. Communication: UV Photoionization of Cytosine Catalyzed by Ag⁺. *J. Chem. Phys.* **2015**, *143* (4), 041103. <https://doi.org/10.1063/1.4927469>.
- (27) Taccone, M. I.; Cruz-Ortiz, A. F.; Dezalay, J.; Soorkia, S.; Broquier, M.; Grégoire, G.; Sánchez, C. G.; Pino, G. A. UV Photofragmentation of Cold Cytosine–M⁺ Complexes (M⁺: Na⁺, K⁺, Ag⁺). *J. Phys. Chem. A* **2019**, *123* (36), 7744–7750. <https://doi.org/10.1021/acs.jpca.9b06495>.

- (28) Broquier, M.; Soorkia, S.; Grégoire, G. A Comprehensive Study of Cold Protonated Tyramine: UV Photodissociation Experiments and Ab Initio Calculations. *Phys. Chem. Chem. Phys.* **2015**, *17* (39), 25854–25862. <https://doi.org/10.1039/C5CP01375E>.
- (29) Kang, H.; Féraud, G.; Dedonder-Lardeux, C.; Juvet, C. New Method for Double-Resonance Spectroscopy in a Cold Quadrupole Ion Trap and Its Application to UV–UV Hole-Burning Spectroscopy of Protonated Adenine Dimer. *J. Phys. Chem. Lett.* **2014**, *5* (15), 2760–2764. <https://doi.org/10.1021/jz5012466>.
- (30) Frisch, M. J.; Trucks, G. W.; Chlegel, H. B.; Scuseria, G. E.; Robb, M. A.; Cheeseman, J. R.; Scalmani, G.; Barone, V.; Petersson, G. A.; Nakatsuji, H.; Li, X.; Caricato, M.; Marenich, A. V.; Bloino, J.; Janesko, B. G.; Gomperts, R.; Mennucci, B.; Hratchian, H. P.; Ortiz, D. J.; Izmaylov, A. F.; Sonnenberg, J. L.; Williams-Young, D.; Ding, F.; Lipparini, F.; Egidi, F.; Goings, J.; Peng, B.; Petrone, A.; Henderson, T.; Ranasinghe, D.; Zakrzewski, V. G.; Gao, J.; Rega, N.; Zheng, G.; Liang, W.; Hada, M.; Ehara, M.; Toyota, K.; Fukuda, R.; Hasegawa, J.; Ishida, M.; Nakajima, T.; Honda, Y.; Kitao, O.; Nakai, H.; Vreven, T.; Throssell, K.; Montgomery, J. A., Jr.; Peralta, J. E.; Ogliaro, F.; Bearpark, M. J.; Heyd, J. J.; Brothers, E. N.; Kudin, K. N.; Staroverov, V. N.; Keith, T. A.; Kobayashi, R.; Normand, J.; Raghavachari, K.; Rendell, A. P.; Burant, J. C.; Iyengar, S. S.; Tomasi, J.; Cossi, M.; Millam, J. M.; Klene, M.; Adamo, C.; Cammi, R.; Ochterski, J. W.; Martin, R. L.; Morokuma, K.; Farkas, O.; Foresman, J. B.; Fox, D. J. Gaussian 16, Revision C.01. Gaussian, Inc., Wallingford CT, 2016.
- (31) Andrae, D.; Häußermann, U.; Dolg, M.; Stoll, H.; Preuß, H. Energy-Adjusted Ab Initio Pseudopotentials for the Second and Third Row Transition Elements. *Theor. Chim. Acta*

- 1990**, 77 (2), 123–141. <https://doi.org/10.1007/BF01114537>.
- (32) TURBOMOLE V7.1, a Development of University of Karlsruhe and Forschungszentrum Karlsruhe GmbH, 1989-2007, TURBOMOLE GmbH, since 2007; Available from [Http://Www.Turbomole.Com](http://www.turbomole.com).
- (33) Western, C. M. PGOPHER: A Program for Simulating Rotational, Vibrational and Electronic Spectra. *J. Quant. Spectrosc. Radiat. Transf.* **2017**, 186, 221–242. <https://doi.org/10.1016/j.jqsrt.2016.04.010>.
- (34) Zhou, C.; Matsika, S.; Kotur, M.; Weinacht, T. C. Fragmentation Pathways in the Uracil Radical Cation. *J. Phys. Chem. A* **2012**, 116 (37), 9217–9227. <https://doi.org/10.1021/jp209213e>.
- (35) Segarra-Martí, J.; Tran, T.; Bearpark, M. J. Ultrafast and Radiationless Electronic Excited State Decay of Uracil and Thymine Cations: Computing the Effects of Dynamic Electron Correlation. *Phys. Chem. Chem. Phys.* **2019**, 21 (26), 14322–14330. <https://doi.org/10.1039/c8cp07189f>.